Appl. Math. and Comp. Sci., 1998, Vol.8, No.2, 213–251

ACTIVE NOISE AND VIBRATION CONTROL

STEPHEN J. ELLIOTT*

Active control can reduce sound and vibration by destructive interference between the original, primary, field and the field generated by controllable secondary sources. It is most effective at low frequencies, for which the wavelength of the disturbance is comparable with the dimensions of the region being controlled. In this review paper the physical limitations of performance are first explored for vibration on a plate and sound in an enclosure, and the nature of the plant response is discussed in these two cases. Adaptive feedforward control algorithms have been successfully used in active control, and these are discussed in terms of an equivalent feedback control system. Finally, the feedback control of sound and vibration is discussed, from the point of view of Internal Model Control, emphasising the importance of plant delay in determining optimal performance, and the trade-off between disturbance rejection and robust stability.

1. Introduction

Sound and vibration have conventionally been controlled using passive methods which involve absorbing the disturbance or blocking its transmission. These methods generally work well at high frequencies, where the wavelength of the disturbance is small compared with the structure or enclosure, but are less effective at low frequencies. At 100 Hz, for example, the wavelength of a soundwave under normal conditions in air is about 3.4 m, and it is difficult to absorb such a sound wave with a thin layer of absorbent material on the walls of an enclosure.

Active sound and vibration control exploits the long wavelengths associated with low frequency disturbances. It works on the principle of destructive interference between the original "primary" soundfield and that due to a number of controllable "secondary" sources. The secondary sources are generally adjusted to minimise the disturbance measured at a number of discrete sensors and a knowledge of the physics of the sound or vibration field is used to ensure that controlling the field at these points leads to attenuation over some useful region of the field. The main physical elements of an active control system are illustrated in Fig. 1, which shows a system acted upon by a number of primary and secondary sources. The signals driving the secondary sources are adjusted to minimise a cost function derived from measurements made on the system which can either give an indication of the system's global or local response.

* University of Southampton, Institute of Sound & Vibration Research, Highfield, Southampton SO17 1BJ, U.K., e-mail: sje@isvr.soton.ac.uk.

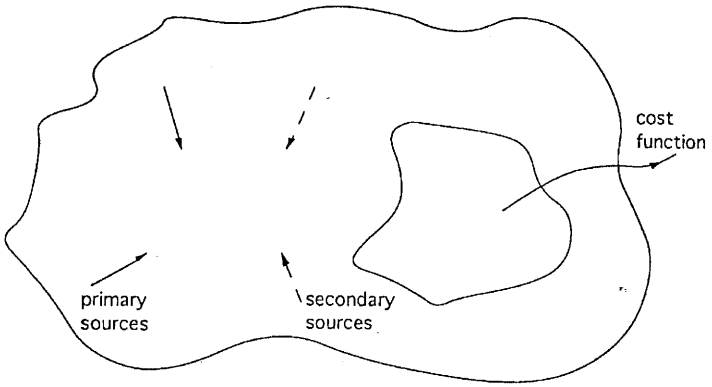

Fig. 1. The physical elements of an active control system.

Although the principle of active noise control dates back to 1936 (Lueg, 1936), and manually adaptive analogue control systems were developed in the 1950's (Conover, 1956), the modern era of active control was spurred by the availability of affordable DSP processors which allowed adaptive multichannel digital controllers to be implemented.

The effective implementation of an active control system relies on an understanding of both the electrical control issues involved (Elliott and Nelson, 1993) and the physics of either the acoustic or structural system being controlled (Nelson and Elliott, 1992; Fuller *et al.*, 1996).

In this review paper the physical limitations on the performance of an active sound or vibration control system are first illustrated by considering both the minimisation of total energy and the creation of a zone of quiet for the vibration on a plate and the sound inside an enclosure. This clearly shows that there is a frequency above which active control cannot generally be usefully applied, which depends on either the size of the whole system or the size of the zone of quiet compared with the wavelength of the disturbance.

The control issues are then introduced by considering two examples of the plant response in active control systems. The first system is for the control of vibration on a plate, and this shows clearly modal behaviour over a wide range of frequencies. The second system considered is the response between a secondary loudspeaker and a microphone in an acoustically well-damped enclosure such as a car interior. Although the response in this case can be described in terms of a modal summation, the separation between the modes is so small compared with the bandwidth that the frequency response does not have resonant peaks.

In many cases where active control can be used to control low frequency sound or vibration, the disturbance is originally generated by a rotating or a reciprocating ma-

chine. The measured disturbance is almost periodic for these cases, and its frequency can be readily measured using a tachometer on the machine, for example. Feedforward methods have been widely used for active control systems in such applications, with an external reference signal derived from the tachometer being used to drive the secondary sources via a controller which is adapted to minimise the disturbance measured at a number of error sensors (Elliott and Nelson, 1993). The algorithms used to adjust these adaptive feedforward controllers were developed from those used in numerical optimisation or adaptive signal processing, but will be analysed here in terms of an exactly equivalent feedback system. This illustrates the "closed loop" nature of adaptive feedforward control and also suggests how the tools of modern feedback control theory can be used to improve the performance and robustness of these algorithms. It also demonstrates how the stability of such adaptive controllers can be proved with relatively few, well defined, assumptions. For broadband disturbances propagating in a clearly defined direction, a reference signal can often be obtained from a detection sensor close to the primary noise source, which provides useful time-advanced information about the disturbance to be cancelled. Adaptive feedforward controllers have thus been extensively used for the active control of random sound propagating in ducts, for example (Eriksson *et al.*, 1987).

Finally, the active control of random disturbances will be discussed for the case in which no external reference signal is available and so a feedback control strategy must be used. It is difficult, for example, to obtain reliable reference signals if the disturbance is generated by numerous uncorrelated primary sources spatially distributed around the point at which control is required. An important example of such a case is the sound generated by the turbulent boundary layer in an aircraft, which is due to a very large number of eddies in the airstream outside the aircraft, each producing their own random contributions. Analogue feedback controllers have previously been used to control the sound inside active headsets and there is considerable interest at the moment in being able to extend such feedback methods to control random soundfields over larger regions of space. The aim of such a feedback control system is the rejection of the disturbances due to the primary sources, rather than tracking of a set point or desired signal. Feedback systems for the active control of sound and vibration are analysed here using the Internal Model Control architecture (Morari and Zafiriou, 1989). This allows the important trade-offs between performance and robustness to be explored and also provides a very convenient method of calculating the disturbance attenuation which can be optimally achieved with various delays in the plant. In practice, this will determine the maximum distance between the secondary source and the error sensor in an active control system and thus the physical size of the region which can be actively controlled.

2. Physical Limits to Active Control

In this section the physical limitations of two active control strategies will be illustrated for both the active control of vibration on a plate, and the active control of sound in an enclosure. Because we are interested in the ultimate physical limitations of these strategies, the electrical control problem will be made as simple as possible

by assuming that the disturbance is tonal and of known frequency, so that only the amplitude and phase of the secondary source(s) need be adjusted at any one frequency to minimise a physically motivated cost function.

2.1. Active Control of Vibrational Kinetic Energy on a Plate

The complex out-of-plane velocity at a point (x, y) on a plate can be expressed as a modal series, for steady state excitation at frequency ω as (Fuller *et al.*, 1996)

$$v(x, y, \omega) = \sum_{n=1}^{\infty} a_n(\omega)\phi_n(x, y) \tag{1}$$

where $a_n(\omega)$ is the complex amplitude and $\phi_n(x, y)$ is the corresponding mode shape of the n-th mode. The structural modes are assumed to be orthogonal and normalised so that

$$\frac{1}{S}\int_S \phi_n(x, y)\phi_m(x, y)\,\mathrm{d}x\,\mathrm{d}y = \begin{cases} 1 & \text{if} \quad n = m \\ 0 & \text{if} \quad n \neq m \end{cases} \tag{2}$$

where S is the surface area of the plate.

The total structural kinetic energy stored in the plate is given by the surface integral over the plate area of half the local mass multiplied by the mean square velocity, which for a uniform plate can be written as

$$E_k(\omega) = \frac{M}{4S}\int_S v^*(x, y, \omega)v(x, y, \omega)\,\mathrm{d}x\,\mathrm{d}y \tag{3}$$

where M is the total plate mass.

If the complex velocity is expressed in terms of the modal series (1), and using the orthonormal property of the modes, the total kinetic energy can also be expressed as

$$E_k(\omega) = \frac{M}{4}\sum_{n=1}^{\infty} |a_n(\omega)|^2 \tag{4}$$

i.e. is proportional to the sum of the modules squared mode amplitudes. To represent realistic physical systems, the summation can be truncated to a finite number of modes with arbitrarily small error. It is the total kinetic energy which is used here as a global measure of the response of the plate.

When the plate is excited by a primary force distribution and M secondary point forces, $f_{s1}, \ldots, f_{sM}$, then the complex amplitude of the n-th mode can be written as

$$a_n(\omega) = a_{np}(\omega) + \sum_{m=1}^{M} B_{nm} f_{sm} \tag{5}$$

where B_{nm} is the coupling coefficient between the m-th actuator and n-th mode, which is proportional to $\phi_n(x, y)$ at the point of application of the m-th secondary force.

Since a finite number of modes are assumed, eqn. (5) can be written in vector terms as

$$\boldsymbol{a} = \boldsymbol{a}_p + \boldsymbol{B}\boldsymbol{f}_s \tag{6}$$

where $a_{np}(\omega)$ is the amplitude of the n-th mode due to the primary force distribution and $\boldsymbol{B}$ is the matrix of coupling coefficients.

The total structural kinetic energy can now be written as

$$E_k = \frac{M}{4}\boldsymbol{a}^H\boldsymbol{a} = \frac{M}{4}\left[\boldsymbol{f}_s^H\boldsymbol{B}^H\boldsymbol{B}\boldsymbol{f}_s + \boldsymbol{f}_s^H\boldsymbol{B}^H\boldsymbol{a}_p + \boldsymbol{a}_p^H\boldsymbol{B}\boldsymbol{f}_s + \boldsymbol{a}_p^H\boldsymbol{a}_p\right] \tag{7}$$

where ^{H} denotes the Hermitian, complex conjugate, transpose. E_k is thus a Hermitian quadratic function of the real and imaginary parts of each of the secondary forces. This is guaranteed to have a global minimum, since the matrix $\boldsymbol{B}^H\boldsymbol{B}$ must be positive definite, which is obtained for a secondary force vector of

$$\boldsymbol{f}_s(\text{opt}) = -\left[\boldsymbol{B}^H\boldsymbol{B}\right]^{-1}\boldsymbol{B}^H\boldsymbol{a}_p \tag{8}$$

which results in a minimum value of kinetic energy given by

$$E_k(\text{min}) = \frac{M}{2}\boldsymbol{a}_P^H\left[\boldsymbol{I} - \boldsymbol{B}\left[\boldsymbol{B}^H\boldsymbol{B}\right]^{-1}\boldsymbol{B}^H\right]\boldsymbol{a}_p \tag{9}$$

Thus, given the primary force distribution, the properties and boundary conditions of the plate, from which the mode shapes can be calculated, and the positions of the secondary sources, the minimum possible total kinetic energy can be calculated after active control for each of a set of discrete excitation frequencies.

Figure 2 shows the physical arrangement for a computer simulation of active minimisation of total kinetic energy on a plate. The steel plate was assumed to have dimensions 380 mm × 300 mm × 1 mm thick, with an internal loss factor of 1% of critical damping and to be simply supported at the edges.

The total kinetic energy of the plate due only to the primary point force, f_p, positioned at $(x, y) = (270, 342)$ mm, is plotted for a range of discrete excitation frequencies as the solid line in Fig. 3. The dashed line shows the level of total kinetic energy after it has been minimised using a single secondary force, f_{s1}, at (30,38) mm and the dashed-dotted line shows the level after minimisation with this and two additional secondary forces, f_{s2} and f_{s3}, at (30,342) mm at (270,38) mm. These results have been obtained by minimising the total kinetic energy at a large number of individual discrete frequencies over the frequency range shown. This represents the limits of performance due only to the physical aspects of the active control problem, and the performance with a practical control system operating on a more complicated primary waveform will inevitably be worse than this. The positions of the primary and secondary sources close to the corners of the plate were chosen to enable them to couple into all the low order structural modes of the plate within this bandwidth. The single secondary force is clearly able to suppress the resonant response of individual modes of the plate below about 200 Hz. Above this frequency several modes with similar natural frequencies can be simultaneously excited by the primary source, when

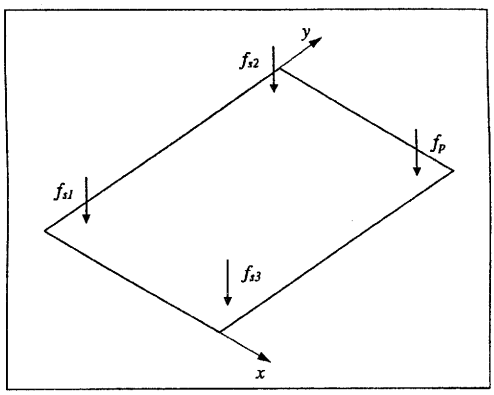

Fig. 2. Physical arrangement for active control of vibration on a plate by a primary point force, f_p, near one corner and either a single secondary point force, f_s, near the opposite corner.

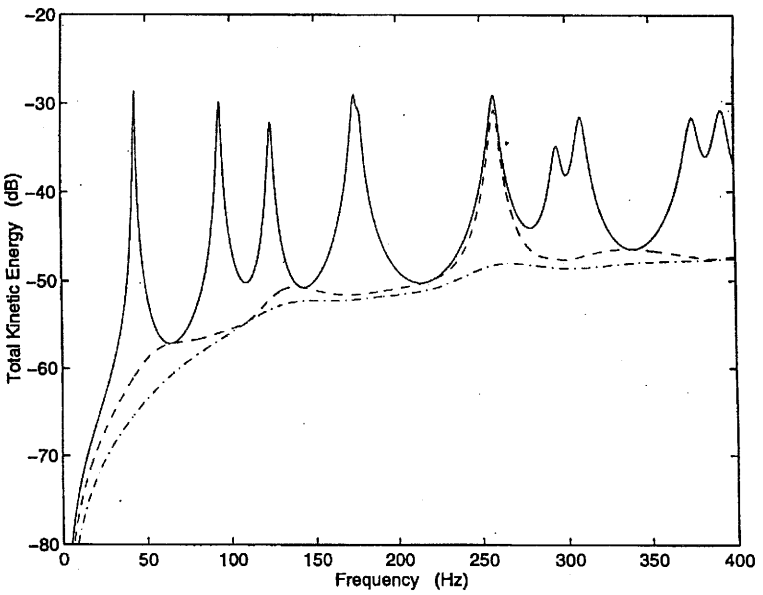

Fig. 3. Total kinetic energy of vibration on a plate when driven by the primary point force, f_p, alone at discrete frequencies (solid line) and after the total kinetic energy has been minimised by a single secondary force, f_{s1}, optimally adjusted at each excitation frequency (dashed line) or three secondary forces, f_{s1}, f_{s2} and f_{s3}, optimally adjusted at each excitation frequency (dash-dot line).

driven at 280 Hz for example, which cannot all be controlled by this single primary source. The use of three secondary forces solves this problem since the combination of secondary forces can independently couple into the two modes contributing to the primary response at 260 Hz and thus achieve control. Notice, however, that between the frequencies at which the resonant responses occur, relatively small reductions in energy can be achieved because of the large number of modes which contribute to the response at these frequencies.

2.2. Active Control of Total Acoustic Potential Energy in an Enclosure

The complex pressure in an enclosure due to an acoustic source distribution operating at a single frequency can be represented by a modal summation exactly analogous to eqn. (1) (Nelson and Elliott, 1992). The total acoustical potential energy in such an enclosure is proportional to the space average mean square pressure and can be written as

$$E_p(\omega) = \frac{1}{4\rho_0 c_0^2} \int_V \left| p(x, y, z, \omega) \right|^2 \mathrm{d}V \tag{10}$$

where ρ_0 and c_0 are the density and speed of sound in the medium, $p(x, y, z, \omega)$ is the complex acoustic pressure at the point (x, y, z) and at the frequency ω in the enclosure and V is the total volume of the enclosure. The total acoustic potential energy provides a convenient cost function for evaluating the effect of global active control of sound in an enclosure.

Because of the assumed orthonormality of the acoustic modes, E_p can again be shown to be proportional to the sum of the squared mode amplitudes, and these mode amplitudes can again be expressed in terms of the contribution from the primary and secondary sources, as in eqn. (6). Thus the total acoustic potential energy is a Hermitian quadratic function of the complex strengths of the secondary acoustic sources, which can be minimised in exactly the same way as described above.

A simulation has been carried out of minimising the total acoustic potential energy in an enclosure of dimensions $1.9 \times 1.1 \times 1.0$ m as illustrated in Fig. 4, in which the acoustic modes have an assumed damping ratio of 10% of critical, which is fairly typical for a reasonably well damped acoustic enclosure such as a car interior at low frequencies. Figure 5 shows the total acoustic potential energy in the enclosure when driven by only the primary source placed in one corner of the enclosure and when the total acoustic potential energy is minimised by a single secondary acoustic source in the opposite corner (dashed line) or by seven secondary acoustic sources positioned at each of the corners of the enclosure not occupied by the primary source (dash-dot line). The positions of the secondary sources were chosen to allow them to couple into the acoustic modes within the enclosure (Nelson and Elliott, 1992). Better active control performance could be obtained if a secondary source was positioned very close to the primary source, but only because of the unrealistic assumption that the primary source only acts at a point in this example.

In this case the response of the system does not show clear modal behaviour for excitation frequencies above about 150 Hz, and very little attenuation can be achieved

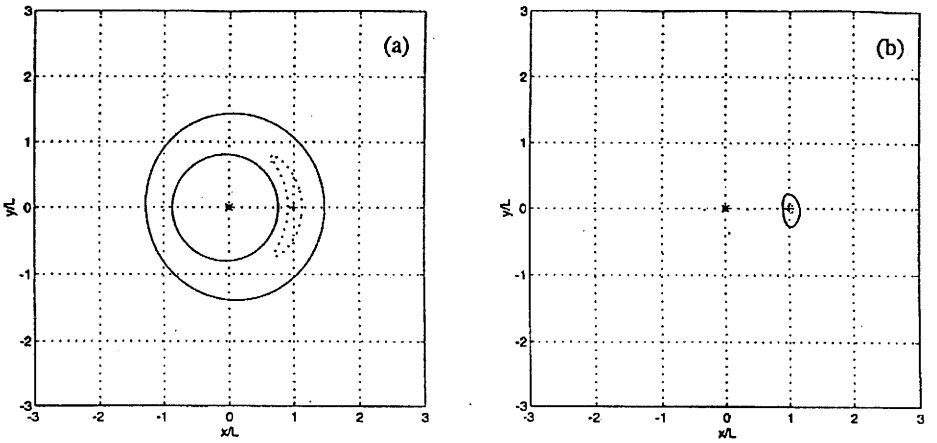

Fig. 8. The spatial extent of the acoustic "zone of quiet" generated by cancelling the pressure at $x/L = 1$ in a three dimensional free field using a point monopole acoustic secondary source at the origin of the co-ordinate system for (a) $L = 0.03\lambda$ and (b) $L = 0.3\lambda$ where λ is the acoustic wavelength. The solid line corresponds to a 10 dB attenuation in the diffuse primary field, and the dashed line to a 20 dB attenuation.

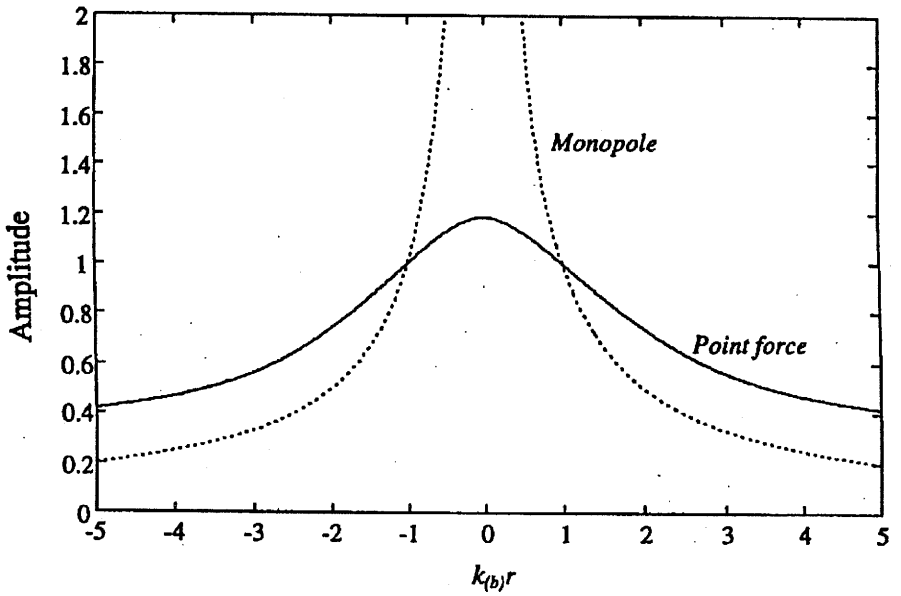

Fig. 9. The near-field velocity due to a point force acting on an infinite plate (solid line) and the near-field pressure due to an acoustic monopole source in free space (dashed line).

a "shell" of cancellation. At higher frequencies in the acoustic case, when $L \geq \lambda/10$, then the zone of quiet does not form a complete shell but is concentrated in a sphere centred on the cancellation point, whose diameter is about $\lambda/10$ (Elliott *et al.*, 1988a; 1988b).

The advantage of a local control system is that the secondary source does not have to drive very hard to achieve control, because it is very well coupled to the response at the cancellation point. Local zones of quiet can often thus be generated without significantly affecting the overall energy in the system.

At low frequencies, where the wavelength of the disturbance is comparable to the dimensions of the system under control, then global active control is feasible, and at higher frequencies it is still possible to achieve local active control over a region of the system which is small compared to the wavelength of the disturbance.

3. Plant Response

In order to allow active control systems to be easily adapted, they are often implemented "digitally", i.e. as a sampled data system. Because the frequencies being controlled are relatively low in audio terms, as explained above, any distortion generated by the digital to analogue converters would occur in a frequency region in which the ear is particularly sensitive and so this is generally avoided by the use of analogue reconstruction filters. Similarly, analogue anti-aliasing filters are generally used to remove disturbances above half the sample rate before digital to analogue conversion, which would otherwise cause audible distortion. If driven by an analogue pure tone, the digital controller and data filters in this case thus only produce an analogue pure tone response and so act linearly with respect to the outside world. Hence the full theory of sample data-systems, with a transformation from the s domain to the z domain which includes aliased components (Franklin *et al.*, 1990), does not need to be used in this case, since aliasing is specifically prevented, and the sampled version of the sensor signals can be taken as a reasonably complete representation of these signals within the bandwidth of the controller. The disadvantage of using these anti-aliasing and reconstruction filters is their significant group delay, which contributes to the overall delay in the plant and can become comparable with the physical delays in the system under control.

The plant response in a digital active control system is assumed to include all of these analogue filters, together with the dynamic response of the secondary actuator and disturbance sensor, and the structural or acoustic response of the physical system under control. The measured plant responses from two examples of active control systems are presented here to illustrate the typical differences between a structural and an acoustic response.

Figure 10 shows the measured frequency response and impulse response of an aluminium plate excited by a small piezoceramic (PZT) actuator bonded to one side of the plate and measured using a distributed piezoelectric (PVDF) film sensor, designed to measure the net volume displacement of the plate (Johnson and Elliott, 1995). In this example of a structural response the response of individual modes can be clearly

seen over the whole frequency range, because the modal overlap is relatively low in this case, as discussed in Section 2. The impulse response has a strong reverberant component and continues at a significant level for about 90 ms.

For many control algorithms the plant response must be internally modelled by the controller. For the structural response shown in Fig. 10 a recursive (IIR) model is clearly appropriate and it was found that when sampled at 2 kHz an acceptable model could be designed with 24 direct and 24 recursive coefficients, whereas 180 coefficients would be required for an FIR filter of comparable accuracy.

Figure 11 shows the frequency responses and impulse response measured from a loudspeaker, acting as a secondary actuator, to a pressure microphone, acting as a disturbance sensor, inside the passenger cabin of a car. In contrast to the structural case, there is almost no modally resonant component in this frequency response. The acoustic enclosure is very heavily damped in this case and the most noticeable features are the zeros in the frequency response, caused by interference between the various acoustic modes at the location of the microphone. The impulse response shows a delay of about 5 ms which is partly due to acoustic propagation time and partly due to delays in the analogue data conversion filters. Most noticeable, however, is the short duration of the impulse response compared with the structural case. The impulse response in Fig. 11(c) is concentrated in a region from about 5 ms to 30 ms. The sampling frequency of the control system in this case was 1 kHz and an accurate model of the plant could be obtained with only 25 coefficients by directly modelling the impulse response with an FIR filter. Such a filter is unconditionally stable and it is very easy to directly adapt its coefficients, which makes it well suited to rapid system identification (Widrow and Stearns, 1985).

4. Adaptive Feedforward Control

Adaptive feedforward methods are very widely used in active control to reject periodic disturbances of known frequency. The algorithms which are used in these adaptive systems generally have their origins in either the signal processing literature (Widrow and Stearns, 1985) or the numerical optimisation literature (Press *et al.*, 1986), and operate in either the time domain or the frequency domain. Some of these algorithms will be described in this section, together with an interpretation of their behaviour in terms of an equivalent feedback controller.

4.1. Frequency Domain Algorithms

We begin with the simple case of a single channel, SISO, controller adapted in the frequency domain using the steepest descent algorithm to reject a tonal disturbance. The block diagram of such a system is shown in Fig. 12 and we will initially assume that the disturbance, $d(j\omega_0)$, is stationary and any transients in the plant caused by a prior change have died away, so the plant is operating in its steady state and can be characterised by its complex response at the excitation frequency ω_0 only, which is $G(j\omega_0)$. The complex error signal under these conditions is thus given by

$$e(j\omega_0, n) = d(j\omega_0) + G(j\omega_0)u(j\omega_0, n) \tag{13}$$

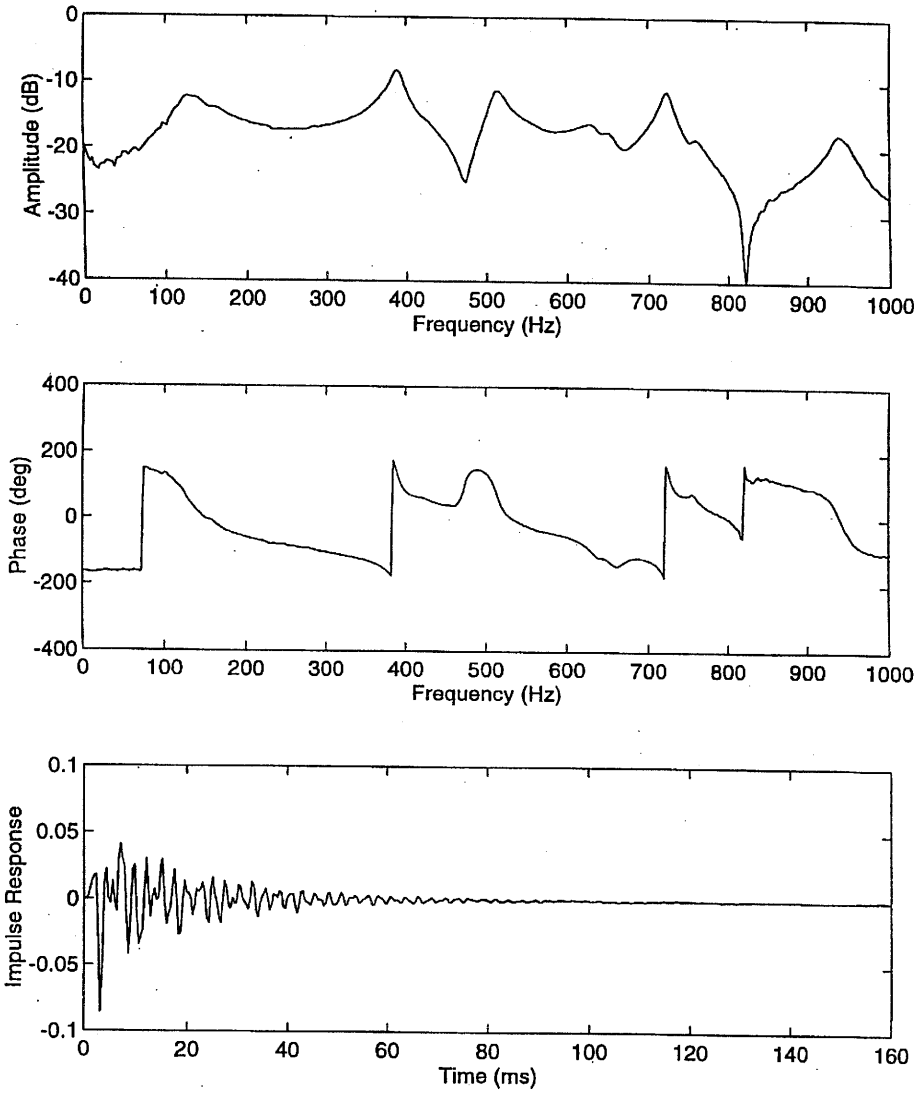

Fig. 10. The modulus and phase of the frequency response of an aluminium plate excited by a piezoceramic actuator and measured using a distributed piezoelectric film sensor. The impulse response of the system is also shown.

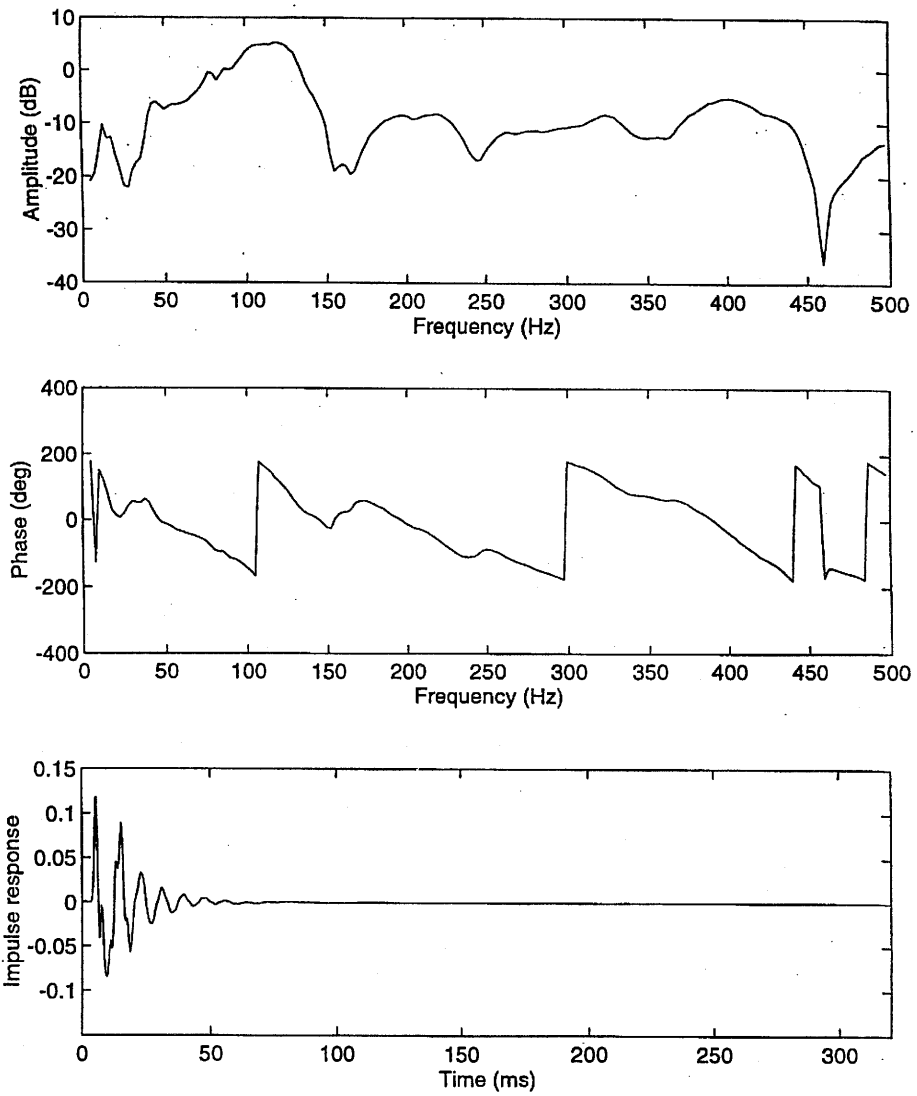

Fig. 11. The modulus and phase of the frequency response of an acoustic enclosure excited by a loudspeaker and measured using a pressure microphone. The impulse response of the system is also shown.

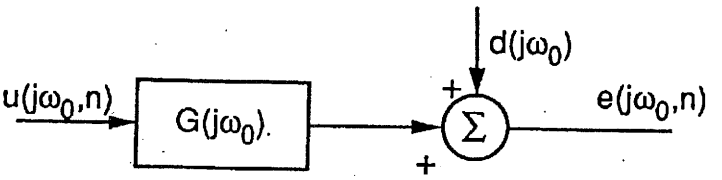

Fig. 12. Block diagram of a single channel feedforward control system operating at a single frequency, ω_0.

where $u(j\omega_0, n)$ is the complex input to the plant from the controller at the n-th iteration of the controller.

The modulus squared error is a quadratic function of the real and imaginary parts of $u(j\omega_0, n)$ with a unique global minimum. The complex gradient of this quadratic function can be defined to be (Elliott and Nelson, 1993)

$$\frac{\partial |e(j\omega_0, n)|^2}{\partial \operatorname{Re}\left(u(j\omega_0, n)\right)} + j\frac{\partial |e(j\omega_0, n)|^2}{\partial \operatorname{Im}\left(u(j\omega_0, n)\right)} = 2G^*(j\omega_0)e(j\omega_0, n) \tag{14}$$

where the (real) derivatives with respect to the real and imaginary parts have been gathered together into a single complex number for convenience and * denotes conjugation. Note that we are not using a derivative with respect to a complex number and so the problems associated with the cost function not being analytic (see e.g. Haykin, 1996, Appendix B) are avoided. If the real and imaginary parts of $u(j\omega_0, n)$ are now adjusted using the method of steepest descents then using (14) the update algorithm can be written as

$$u(j\omega_0, n+1) = u(j\omega_0, n) - \alpha \hat{G}^*(j\omega_0)e(j\omega_0, n) \tag{15}$$

where α is a (real) adaptation coefficient, and $\hat{G}(j\omega_0$ is an estimate of the complex plant response used by the adaptive algorithm.

It could be argued that if the error is given by eqn. (13), and the plant estimate $\hat{G}(j\omega_0)$ was perfectly accurate, then $e(j\omega_0, n+1)$ could be set to zero in one iteration by using the algorithm

$$u(j\omega_0, n+1) = u(j\omega_0, n) - \hat{G}^{-1}(j\omega_0)e(j\omega_0, n) \tag{16}$$

Notice, however, that the phase of $\hat{G}^{-1}(j\omega_0)$ is the same as that of $\hat{G}^*(j\omega_0)$ and if $a = (|\hat{G}(j\omega_0)|^2)^{-1}$ in eqn. (15), it is identical to eqn. (16). In the SISO case the iterative exact least squares solution is thus obtained as a special case of the steepest descent algorithm, with a particular value of convergence coefficient.

We now consider the sequence of complex steady state values of $u(j\omega_0, n)$ and $e(j\omega_0, n)$ as a sampled time history, with z transforms $u(z)$ and $e(z)$, and take the z transform of eqn. (15), to give

$$u(z) = \frac{-\alpha}{z-1}\hat{G}^*(j\omega_0)e(z) \tag{17}$$

The adaptive feedforward controller in this case can be interpreted as a fixed feedback controller, sampled at a slow enough rate for the plant transients to die away between sample times. Taking the z transform of eqn. (10), we obtain

$$e(z) = d + Gu(z) \tag{18}$$

The equivalent block diagram for this interpretation of the adaptive feedforward controller is thus of the form shown in Fig. 13, where G is now just a complex gain, and the negative "feedback controller" has the transfer function

$$H(z) = \frac{\alpha}{z-1}\hat{G}^*(j\omega_0) \tag{19}$$

The term $\lambda/(z-1)$ is a digital integrator and so, provided the system is stable, the control loop will exactly compensate for any observed error over a timescale determined by the 'gain' parameter λ.

The function of the term $\hat{G}^*(j\omega_0)$ in eqn. (19) is to compensate for the phase of the plant at the excitation frequency, so that ideally, if $\hat{G}(j\omega_0) = G(j\omega_0)$, the real and imaginary parts of $e(n)$ respond independently. The feedback controller shown in Fig. 13 has a single pole given by

$$z = 1 - \alpha G(j\omega_0)\hat{G}^*(j\omega_0) \tag{20}$$

and will thus be stable providing α is small and positive and the real part of $G(j\omega_0)\hat{G}^*(j\omega_0)$ is positive, which is ensured providing that the phase of $\hat{G}(j\omega_0)$ is within $\pm 90°$ of that of $G(j\omega_0)$, (Elliott *et al.*, 1987; Morgan, 1980).

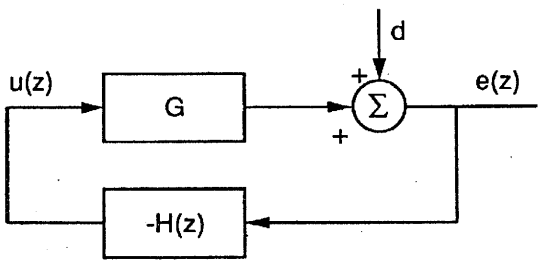

Fig. 13. Equivalent feedback system for the iteratively adapted frequency-domain feedforward algorithm.

Multichannel (MIMO) frequency domain adaptive feedforward control systems can be treated in an exactly analogous way. In this case the vector of complex steady-state error signals at the n-th iteration is given by

$$\boldsymbol{e}(j\omega_0, n) = \boldsymbol{d}(j\omega_0) + \boldsymbol{G}(j\omega_0)\boldsymbol{u}(j\omega_0, n) \tag{21}$$

where $\boldsymbol{G}(j\omega_0)$ is now the matrix of complex responses between each secondary actuator and each error sensor at the excitation frequency. Similarly, the adaptive steepest descent algorithm becomes

$$\boldsymbol{u}(j\omega_0, n+1) = \boldsymbol{u}(j\omega_0, n) - \alpha\hat{\boldsymbol{G}}^H(j\omega_0)\boldsymbol{e}(j\omega_0, n) \tag{22}$$

Taking the z transform of eqn. (22) leads to the equivalent MIMO feedback controller in this case, so that in the z domain the vector of error signals becomes

$$\boldsymbol{e}(z) = \left[\boldsymbol{I} + \boldsymbol{G}\boldsymbol{H}(z)\right]^{-1}\boldsymbol{d}(z) \tag{23}$$

where in this case $\boldsymbol{G}$ is equal to $\boldsymbol{G}(j\omega_0)$ and

$$\boldsymbol{H}(z) = \frac{\alpha}{z-1}\hat{\boldsymbol{G}}^H(j\omega_0) \tag{24}$$

The stability of the MIMO system is governed by the poles of the system. These are the roots of the characteristic equation obtained by setting the determinant of the equation

$$\boldsymbol{I} + \boldsymbol{G}\boldsymbol{H}(z) = \boldsymbol{I} + \frac{\alpha}{z-1}\boldsymbol{G}(j\omega_0)\hat{\boldsymbol{G}}^H(j\omega_0) \tag{25}$$

to zero. The pole positions are thus given by

$$z_i = 1 - \alpha\lambda_i \tag{26}$$

where λ_i is the i-th eigenvalue of $\boldsymbol{G}(j\omega_0)\hat{\boldsymbol{G}}^H(j\omega_0)$. The MIMO system will thus be stable provided $|z_i| < 1$ for all λ_i, which is equivalent to the condition

$$0 < \alpha < \frac{2\,\mathrm{Re}\,(\lambda_i)}{|\lambda_i|^2} \qquad \text{for all} \quad \lambda_i \tag{27}$$

For slow convergence, small α, eqn. (27) implies that for stability the real parts of each of the eigenvalues of $\boldsymbol{G}(j\omega_0)\hat{\boldsymbol{G}}^H(j\omega_0)$ must be positive. This condition has previously been derived (Elliott *et al.*, 1992) from an analysis of the iterative convergence of eqn. (22).

Assuming the plant model is perfect, the iterative algorithm is guaranteed to be stable, for small α, since the eigenvalues of the Hermitian matrix $\boldsymbol{G}(j\omega_0)\,\boldsymbol{G}^H(j\omega_0)$ are either positive or zero. Under these conditions the convergence of the control system can be decomposed into a set of "modes" which each converge independently with a time constant proportional to $1/\lambda_i$ (Elliott *et al.*, 1992). The non-zero eigenvalues of the matrix $\boldsymbol{G}(j\omega_0)\,\boldsymbol{G}^H(j\omega_0)$ calculated from a measured matrix of transfer responses are shown in Fig. 14 (Elliott *et al.*, 1992). The transfer response matrix

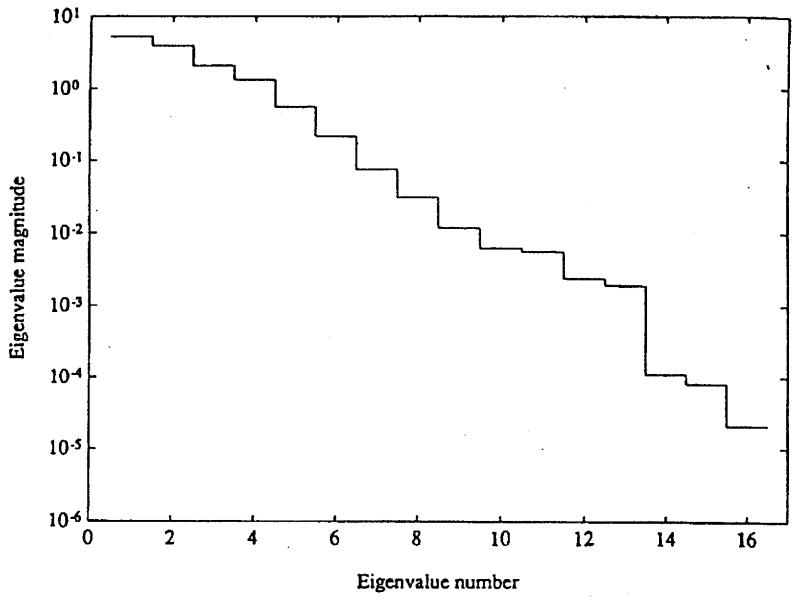

Fig. 14. The eigenvalues of the matrix $\boldsymbol{G}(j\omega_0)\,\boldsymbol{G}^H(j\omega_0)$ for the acoustic transfer response measured from 16 loudspeakers to 32 microphones in an enclosure excited at 88 Hz.

$\boldsymbol{G}(j\omega_0)$ was measured from 16 loudspeakers to 32 microphones in a 6 m × 2.2 m × 2.2 m enclosure at an excitation frequency of 88 Hz. The eigenvalues are entirely real in this case and have a range of about 10^6. The large range of eigenvalues suggests that in this case the system is very ill-conditioned. This is because a larger number of loudspeakers have been used to control the soundfield at this excitation frequency than were necessary from an analysis of the number of acoustic modes being excited. This is a not-uncommon situation in active control, however, where the number of actuators may be chosen to ensure good control under worst-case conditions, e.g. higher frequency excitation, but the system often has to operate under conditions in which the number of actuators is over specified.

An example of the convergence of the sum of the squared errors at the 32 microphones is shown in Fig. 15 for an adaptive feedforward active sound control system operating in this enclosure. Several control modes with large eigenvalues are significantly excited by the primary disturbance and these decay away relatively quickly to give an attenuation of 20 dB in the sum of squared errors. The modes with the smaller eigenvalues die away more slowly, and the sum of squared errors is eventually reduced by more than 30 dB. In practice, however, it is the rapid initial convergence which has the largest subjective effect.

In practice the plant model is not perfect and for systems with large numbers of actuators and sensors it is likely that some of the eigenvalues of $\boldsymbol{G}(j\omega_0)\,\hat{\boldsymbol{G}}^H(j\omega_0)$ will have small negative real parts, which gives rise to slow unstable modes. One method of

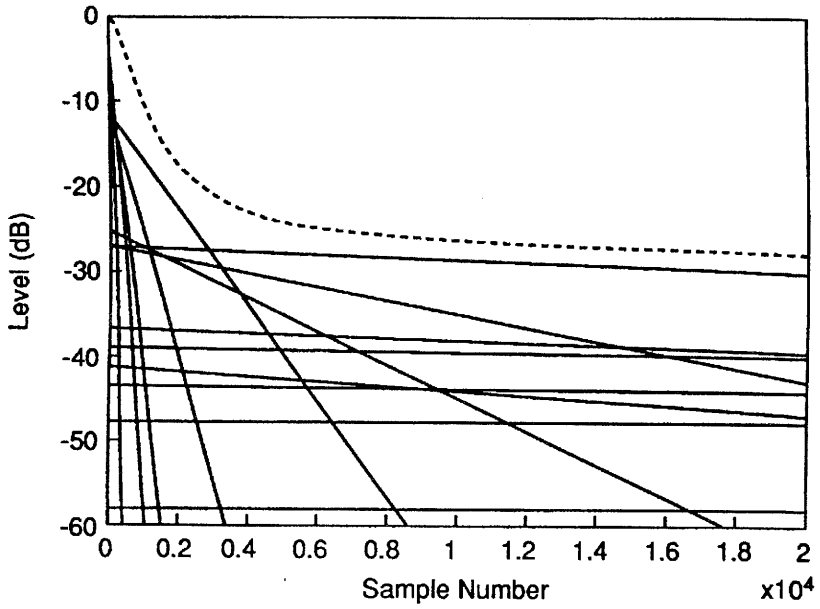

Fig. 15. The level of the reduction in the sum of squared errors against time for the overall convergence of an iterative multichannel feedforward controller controlling the sum of squared errors at 32 microphones with 16 loudspeakers (dashed curve). Also shown is the convergence behaviour of the individual 'modes' of the control system (solid lines).

making the control system more robust to such uncertainty is to implement a steepest descent algorithm which minimises the sum of squared errors and a real parameter, β, times the sum of squared control efforts. Equation (22) then becomes (Elliott *et al.*, 1992)

$$\boldsymbol{u}(j\omega_0, n+1) = (1-\alpha\beta)\boldsymbol{u}(j\omega_0, n) - \alpha\hat{\boldsymbol{G}}^H(j\omega_0)\boldsymbol{e}(j\omega_0, n) \tag{28}$$

which is referred to as a 'leaky' algorithm in the signal processing literature (Widrow and Stearns, 1985). The equivalent feedback controller in this case is equal to

$$\boldsymbol{H}(z) = \frac{\alpha}{z-1+\alpha\beta}\hat{\boldsymbol{G}}^H(j\omega_0) \tag{29}$$

and the perfect digital integrator in eqn. (24) has been replaced by a 'leaky' integrator. The stability of this control system is now determined by the eigenvalues of the matrix $[\boldsymbol{G}(j\omega_0)\hat{\boldsymbol{G}}^H(j\omega_0) + \beta\boldsymbol{I}]$ so that any eigenvalue of $\boldsymbol{G}(j\omega_0)\hat{\boldsymbol{G}}^H(j\omega_0)$ with a small negative real part can be compensated for by an appropriate positive value of β. Even if the plant model is perfect, the effort weighting parameter has the effect of reducing the range of eigenvalues in the control problem, thus reducing any ill-conditioning.

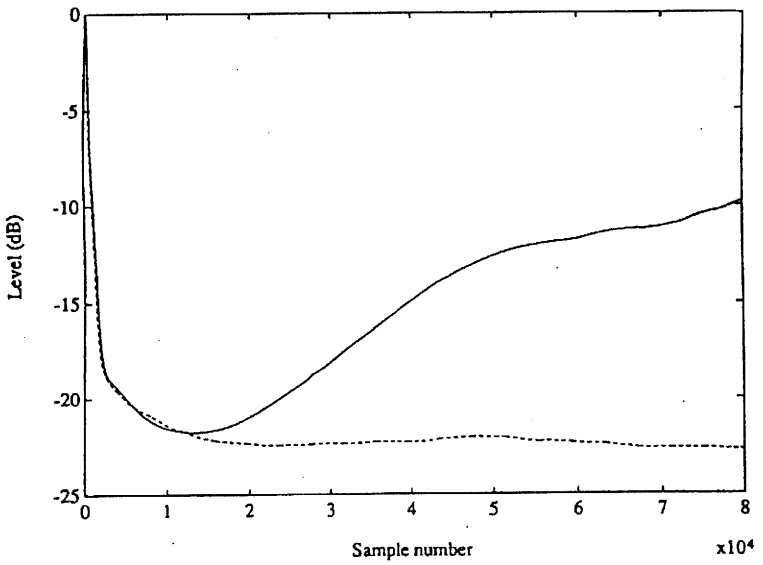

Fig. 16. The level of the sum of squared error signals when an adaptive feedforward control system with errors in the estimated plant response matrix is used to control the tonal disturbance at 32 microphones using 16 loudspeakers with no effort weighting in the cost function (solid line) and when a sufficient effort weighting (β) is included in the cost function to stabilise the system (dashed line).

The convergence behaviour of the multichannel controller described above when rather large random errors were introduced into the matrix $\hat{\boldsymbol{G}}(j\omega_0)$ is shown in Fig. 16 (Elliott *et al.*, 1992). The solid line shows the behaviour with the effort weighting parameter, β, equal to zero, in which case some of the control modes have small negative eigenvalues and are unstable. The unstable behaviour is only evident after the fast initial convergence, however, since the modes associated with the large eigenvalues are relatively unaffected. The exponential increase in the sum of squared errors is limited in practice by saturation of the loudspeaker amplifiers. If a suitable value of effort weighting parameter is included in the adaptive algorithm, the real parts of all the eigenvalues of the $[\boldsymbol{G}(j\omega_0)\hat{\boldsymbol{G}}^H(j\omega_0) + \beta\boldsymbol{I}]$ matrix will be positive and the control system is stabilised, as shown by the dashed line in Fig. 16. This level of β does not significantly affect the larger eigenvalues and thus the initial rapid convergence behaviour is largely unaffected.

If the slow modes of convergence in the steepest descent algorithm are a problem, algorithms based on Gauss-Newton methods could be used. This leads to an iterative algorithm of exactly the same form as eqn. (22) with the pseudo-inverse of the estimated plant response replacing its Hermitian transpose. Assuming there are more error sensors (L) than secondary sources (M), so that the problem is overdetermined, this pseudo-inverse is equal to

$$\hat{\boldsymbol{G}}^{\dagger}(j\omega_0) = \left[\hat{\boldsymbol{G}}^H(j\omega_0)\hat{\boldsymbol{G}}(j\omega_0)\right]^{-1}\hat{\boldsymbol{G}}^H(j\omega_0) \tag{30}$$